Design and Investigation of a High-Sensitivity Tilt Sensor Based on FBG

Jianjun PAN[1], Liangying WANG[2*], Wei HOU[2], and Hanyang LV[3]

[1]*National Engineering Research Center of Fiber Optic Sensing Technology and Networks, Wuhan University of Technology, Wuhan 430070, China*

[2]*School of Mechanical and Electronic Engineering, Wuhan University of Technology, Wuhan 430070, China*

[3]*School of Information Engineering, Wuhan University of Technology, Wuhan 430070, China*

[*]Corresponding author: Liangying WANG E-mail: 2913000150@qq.com

Abstract: In this paper, a high-sensitivity fiber Bragg grating (FBG) tilt sensor using a cantilever-based structure is introduced. Two FBGs are fixed on a specially designed elastomer. One end of the elastomer is connected to the mass block, and the other end is connected to the shell. The principle of the tilt sensor is introduced in detail, and the mathematical model is established. The performance of the sensor is studied. The results show that there is a good linear relationship between the central wavelength difference of the two FBGs and the tilt angle in the range of –5° to 5°. The repeatability of the sensor is good, and the tilt sensitivity can reach 231.7 pm/°. The influence of the silicone oil on the damping capacity of the sensor is studied. The results show that the damping capacity of the sensor has been improved by sealing the silicone oil inside the shell of the sensor. The field test is carried out on a pier of an elevated bridge, and the result is good, which verifies the practicability of the sensor.

Keywords: Tilt sensor; FBG; temperature self-compensation; silicon oil; vibration damping

Citation: Jianjun PAN, Liangying WANG, Wei HOU, and Hanyang LV, "Design and Investigation of a High-Sensitivity Tilt Sensor Based on FBG," *Photonic Sensors*, 2023, 13(2): 230228.

1. Introduction

As an important part of computational science, the angle measurement technology plays a vital role in structural health monitoring and natural disaster warning [1, 2]. Inclinometers for inclination measurement are more and more widely used in various departments and fields such as bridges, geotechnical engineering, and construction [3–7], and the requirements for their measurement accuracy and technical level are also increasing. Most of the traditional tilt sensors are electrical sensors, which have high measurement accuracy and resolution. The principle of electromagnetic inclination measurement is basically to convert the angle into electrical signal by using the effect of the gravity field, but it is vulnerable to electromagnetic interference and has limited transmission distance, which makes it difficult to apply in harsh environments. Fiber Bragg grating (FBG) sensors have been widely used in the field of structural health monitoring due to their advantages of anti-electromagnetic interference, strong stability, small size, and corrosion resistance [8, 9].

Received: 7 June 2022 / Revised: 27 July 2022

DOI: 10.1007/s13320-022-0671-8
Article type: Regular

Several tilt sensors based on the FBG have been reported. It is a widely used method to directly paste the FBG on a cantilever beam to make an inclination sensor. When the beam bends, the FBG perceives the bending deformation of the beam surface. Jiang *et al.* [10], Ma *et al.* [11], and Liang *et al.* [12] reported such sensors. The tilt sensitivity was 9.9 pm/°, 16.17 pm/°, and 31.3 pm/°, respectively. This kind of sensor has the advantages of simple structure and good linearity. However, the high sensitivity is difficult to achieve and the applications in small-angle monitoring environments are limited. Some other tilt sensors have been developed for the high tilt sensitivity. Fu *et al.* [13] proposed an omni-azimuth angle sensor for tilt measuring based on the FBG array. The sensor consisted of a mass block and a cube frame connected by an FBG array. The angle sensitivity varied unevenly with the tilt angle and the range of variation was 80 pm/° to 459.3 pm/°. However, the fabrication process of the sensor was complex and the calibration was difficult. Pan *et al.* [14] proposed a high-resolution optical-fiber tilt sensor by the Fabry-Perot (F-P) filter. The sensor was composed of a pair of optical fiber collimators and a simple pendulum with an F-P filter. Its average sensitivity achieved 1104 pm/°, but it had the disadvantages of poor linearity, complex structure, and poor reusability. Yang *et al.* [15] proposed an FBG tilt sensor with a pendulum-based structure. The sensing head consisted of two FBGs attached on a specially designed columnar pendulum. The tilt sensitivity was 74 pm/°. Maheshwari *et al.* [16] proposed a rotation independent in-place tilt sensor based on the FBG. The optical fiber carried a symmetrical mass body at its midpoint to form the sensor. The tilt sensitivity was 168 pm/°. The above two tilt sensors achieved the high tilt sensitivity. However, the size of these sensors was very large, which was difficult to apply in the conventional engineering applications.

In this paper, an FBG tilt sensor based on the cantilever structure is proposed. By setting a fiber-optic fixing arm at both ends of the elastic steel sheet to form an elastomer, the sensor not only offers the high sensitivity, but also keeps the small size. The sensing characteristics of the proposed sensor are studied. The main static performance indexes of the sensor are good, and the sensitivity can reach 231.7 pm/°, which is higher than those of most FBG tilt sensors. By sealing the silicone oil inside the shell of the sensor, the seismic performance of the sensor is effectively improved. The designed sensor also has the advantages of the compact structure, convenient installation, and temperature compensation, which is suitable for small angle measurement in various environments.

2. Sensor design and analysis

2.1 Structure design of the sensor

An FBG tilt sensor based on a cantilever beam structure is proposed, as shown in Fig. 1. The sensor mainly consists of an elastomer, two FBGs, a mass block, and a shell. The ends of the two FBGs are fixed on the elastomer with epoxy resin. One end of the elastomer is installed on the shell with a screw, and the mass block is installed on the other end of the elastomer with a screw. The mass block and elastomer are made of stainless steel, and the shell is made of aluminum. During the encapsulation process, a pre-stress is applied to the FBGs, which enables the negative strain to be perceived by the FBG. The size of the elastomer is 54 mm × 12 mm × 8 mm.

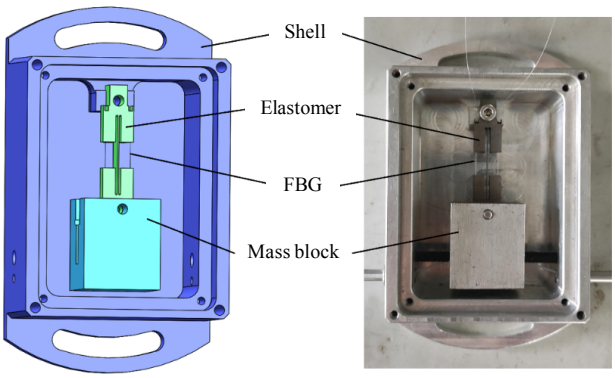

Fig. 1 Structure of the tilt sensor.

When the measured structure is tilted and deformed, one of the two FBGs is stretched, while the other is compressed, resulting in the shifts of the central wavelength of the two FBGs. Therefore, the tilt angle can be monitored through the central wavelength variation of FBGs. Considering that two FBGs are in the same temperature field, the influence of temperature can be eliminated by a differential compensation design, meanwhile, the double sensitivity can be achieved.

The elastomer is the key structure of the sensor. As shown in Fig. 2, the elastomer is composed of the elastic steel sheet and the fiber-optic fixing arm. The fiber-optic fixing arm is set at both ends of the elastic steel sheet, and the FBGs are fixed on the fiber-optic fixing arm. Through the elastomer, the strain on the cantilever surface is amplified twice and transmitted to the FBG. Firstly, in the height direction of the elastomer, according to the mechanics of materials, it can be known that the normal strain of a section is proportional to the distance from the point to the neutral surface when the cantilever beam bends. Compared with the cantilever beam surface, the distance between the optical fiber fixed arm and the neutral layer of the cantilever beam is larger. Therefore, the surface deformation of the fiber-optic fixing arm ΔL_{CD} is larger than the surface deformation of the cantilever beam ΔL_{AB}. Secondly, in the length direction of the elastomer, according to the principle of the strain concentration, it can be known that with the same deformation, the strain perceived by the FBG is inversely proportional to the length of the FBG mount. The length of the FBG mount L_f is less than the distance between Points C and D (ΔL_{CD}), so the strain on the FBG is greater than those at Points C and D. Due to the sensitizing effect of the height and length directions, the sensor realizes the high sensitivity, retains the small size, and effectively avoids the excessive size caused by the long cantilever beam length.

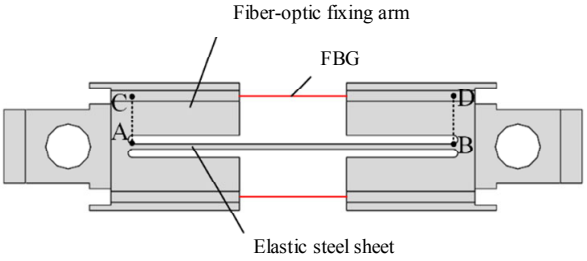

Fig. 2 Structure of the elastomer.

2.2 Theoretical analysis

The working principle of the proposed sensor is shown in Fig. 3, and the elastic steel sheet can be regarded as a cantilever beam. When the cantilever beam bends, although one of the two FBGs is stretched and the other is compressed, the direction of the bending moment exerted on the fixed end of the cantilever beam by the two FBGs is the same. Therefore, the torque balance equation can be expressed as

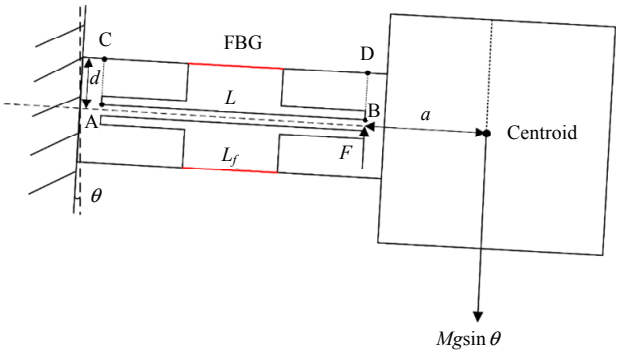

Fig. 3 Working principle of the tilt sensor.

$$mg\sin\theta(a+L)-FL-2k_f\Delta L_f d=0 \qquad (1)$$

where m is the mass of the mass block, g is the acceleration of the gravity, θ is the tilt angle, L is the length of the cantilever beam, ΔL_f is the deformation of the FBG, a is the distance between the centroid of mass and the free end of the cantilever beam, k_f is the elastic coefficient of the FBG, and F is the equivalent force of the free end of cantilever beam. The elastic coefficient of fiber can be given as

$$k_f=\frac{AE_f}{L_f} \qquad (2)$$

where A is the cross-sectional area of the FBG, E_f

is the elastic modulus, and L_f is the length of the optical fiber between the two fixing points.

According to material mechanics, the average strain on the surface of cantilever beam is

$$\varepsilon_1 = \frac{\Delta L_{AB}}{L} = \frac{3FL}{Ebh^2} \tag{3}$$

where ΔL_{AB} is the deformation of the upper surface of the cantilever beam, E is the elastic modulus of the cantilever beam, b is the length of the cantilever beam section, and h is the width of the cantilever beam section.

Figure 4 shows the deformation process of the elastomer. When the bending angle of the elastic steel sheet is $\mathrm{d}\theta$, the surface deformation of the cantilever beam can be represented as

$$\Delta L_{AB} = \overline{A'B'} - \overline{AB} = \left(\rho + \frac{h}{2}\right)\mathrm{d}\theta - \rho\mathrm{d}\theta = \frac{h}{2}\mathrm{d}\theta . \tag{4}$$

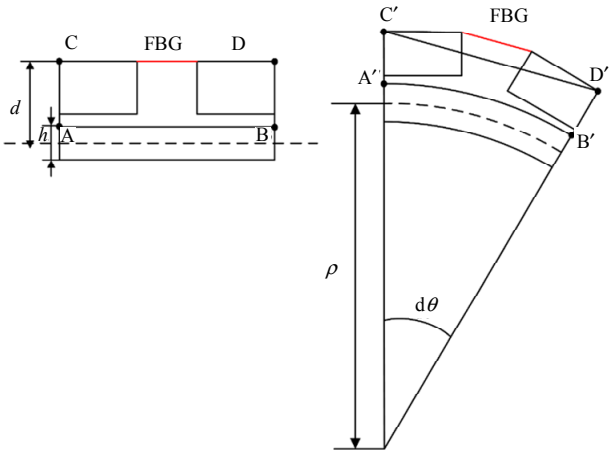

Fig. 4 Deformation process of the elastomer.

The distance variation between Points C and D can be expressed as

$$\begin{aligned}\Delta L_{CD} &= \overline{C'D'} - \overline{CD} \\ &= 2(\rho + d)\frac{\mathrm{d}\theta}{2} - \rho\mathrm{d}\theta = d\mathrm{d}\theta\end{aligned} \tag{5}$$

where d is the distance between the fiber fixed point and the neutral plane of the cantilever beam.

From (4) and (5), it can be seen that the surface deformation of the cantilever beam has been amplified by the fiber-optic fixing arm, and the amplification coefficient is

$$K = \frac{\varepsilon_2}{\varepsilon_1} = \frac{2d}{h} . \tag{6}$$

As the deformation of the fiber-optic fixing arm is much smaller than that of the fiber, there is $\Delta L_f \approx \Delta L_{CD}$. From (1), (2), (3), and (6), ΔL_f can be expressed as

$$\Delta L_f = K\Delta L_{AB} = \frac{mg(a+L)\sin\theta}{\left(\frac{Ebh^3}{6Ld} + 2\frac{AE_f d}{L_f}\right)} . \tag{7}$$

The strain of FBG can be expressed as

$$\varepsilon_2 = \frac{\Delta L_f}{L_f} = \frac{mg(a+L)\sin\theta}{\left(\frac{Ebh^3}{6Ld} + 2\frac{AE_f d}{L_f}\right)L_f} . \tag{8}$$

When the measured structure is tilted, the gravity component of the mass block drives the cantilever beam to bend, so that the FBG is stretched or contracted. The magnitude of the strain on both FBGs is the same. The central wavelength shifts of the two FBGs can be expressed separately as

$$\frac{\Delta\lambda_1}{\lambda_B} = K_T\Delta T + K_\varepsilon\varepsilon_2 \tag{9}$$

$$\frac{\Delta\lambda_2}{\lambda_B} = K_T\Delta T - K_\varepsilon\varepsilon_2 \tag{10}$$

where K_T is the temperature coefficient, K_ε is the strain coefficient, ΔT is the temperature change, and λ_B is the central wavelength of the FBG.

When θ is small, there is $\sin\theta \approx \theta$. From the above (8), (9), and (10), the sensitivity of the sensor can be expressed as

$$S = \frac{\Delta\lambda_1 - \Delta\lambda_2}{\theta} = \frac{2K_\varepsilon mg(a+L)\lambda_B}{\left(\frac{Ebh^3}{6Ld} + 2\frac{AE_f d}{L_f}\right)L_f} . \tag{11}$$

As can be seen from (11), the sensitivity of the sensor is influenced by many parameters. Increasing m or decreasing L_f will significantly improve the sensitivity of the sensor. The sensitivity can also be improved by adjusting key parameters d, L, a, b, and h. In practical engineering applications, the size of the sensor is often limited, and in the case that the size should not be too large, the sensitivity

requirements in different applications can be met by adjusting d and L_f. Figure 5 shows the relationship between the sensitivity and key structural parameters, d and L_f. Based on the theoretical analysis and engineering practice, the parameters of the sensor are shown in Table 1. Taking the optimized parameters into (11), the sensitivity of the sensor can be obtained as 251.4 pm/°. In order to ensure that the tensile strength of the fiber is within a safe range, the measurement range of the sensor is set to – 5° to 5°.

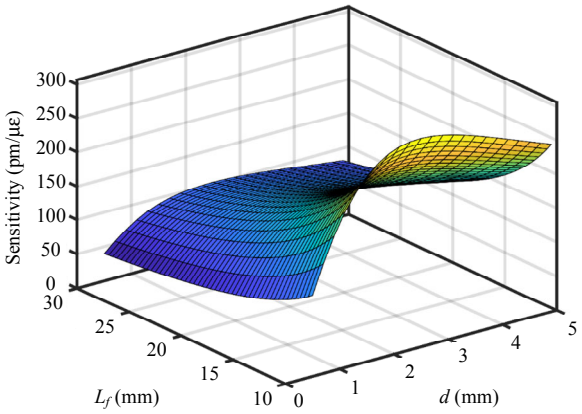

Fig. 5 Relationship between the sensitivity and parameters, L_f and d.

Table 1 Key parameters.

Parameters	Value
Length of the optical fiber between the two fixing points / L_f	10 mm
Diameter of FBG	125 μm
Central wavelength of FBG1 / λ_1	1 534 nm
Central wavelength of FBG2 / λ_2	1 538 nm
Elastic modulus of FBG / E_f	74. 52 GPa
Length of the cantilever beam / L	30 mm
Length of the cantilever beam section / b	8 mm
Width of the cantilever beam section / h	0.5 mm
Distance between the fiber fixing point and the neutral plane of the cantilever beam / d	4.75 mm
Elastic modulus of cantilever beam / E	200 GPa
Distance between the centroid of mass and the free end of cantilever beam / a	15 mm
Mass of the mass block / m	150 g
Gravitational acceleration / g	9.8 m/s^2

2.3 Simulation analysis

Static and dynamic responses of the sensor are simulated using ANSYS. The elastomer and mass block are fixed together by a bonding connection. The mass block is bonded to one end of the elastomer. The FBG is bonded on the elastomer using epoxy resin. Material parameters used in the simulation are shown in Table 2. From (1), it can be calculated that when the tilt angle θ is 1°, the gravity component is about 0.025 6 N, and the two are almost linear in the range of –5° to 5°, so the correspondence between the gravity component and the tilt angle is considered as 0.025 6 N/°. The static analysis is used to analyze the static characteristics of the sensor. One end of the elastomer is fixed, and a vertical force from 0 N to 0.128 N with a step of 0.025 6 N is applied to the centroid of the mass block to simulate the gravity component. The harmonic response analysis is used to analyze the dynamic characteristics of the sensor. One end of the elastomer is fixed, and a vertical simple harmonic force from 0 Hz to 30 Hz with a step of 1 Hz is applied to the centroid of the mass block. The amplitude of the simple harmonic force is 0.025 6 N. The strain of two FBGs is the output and the sensitivity of the sensor is analyzed.

Table 2 Material parameters.

Materials	Elastic modulus (MPa)	Poisson ratio
Elastomer	200	0.3
FBG	74.52	0.17
Epoxy resin	3	0.38

Figure 6 shows the strain cloud with a load of 0.025 6 N. The strain cloud shows that the deformation is almost entirely concentrated on the FBG. Figure 7 shows the strains on the paths of the two FBGs at a load from 0 N to 0.128 N. The results show that the value of the strain on the FBGs increases linearly with an increase in the force. According to the correspondence between the load

and the tilt angle, the correspondence between the strain and the tilt angle on the two FBGs are 99.91 με/° and –99.95 με/°, respectively, so the sensitivity can be obtained after the difference is 199.86 με/°. After the conversion with the wavelength, the calculated simulation sensitivity is 239.8 pm/°. Figure 8 shows the dynamic response results of the sensor. The resonant frequency of the sensor is about 18 Hz, and the effective working frequency range of the sensor is 0 Hz to 10 Hz, which indicates that the sensor is suitable for working in the low frequency environment.

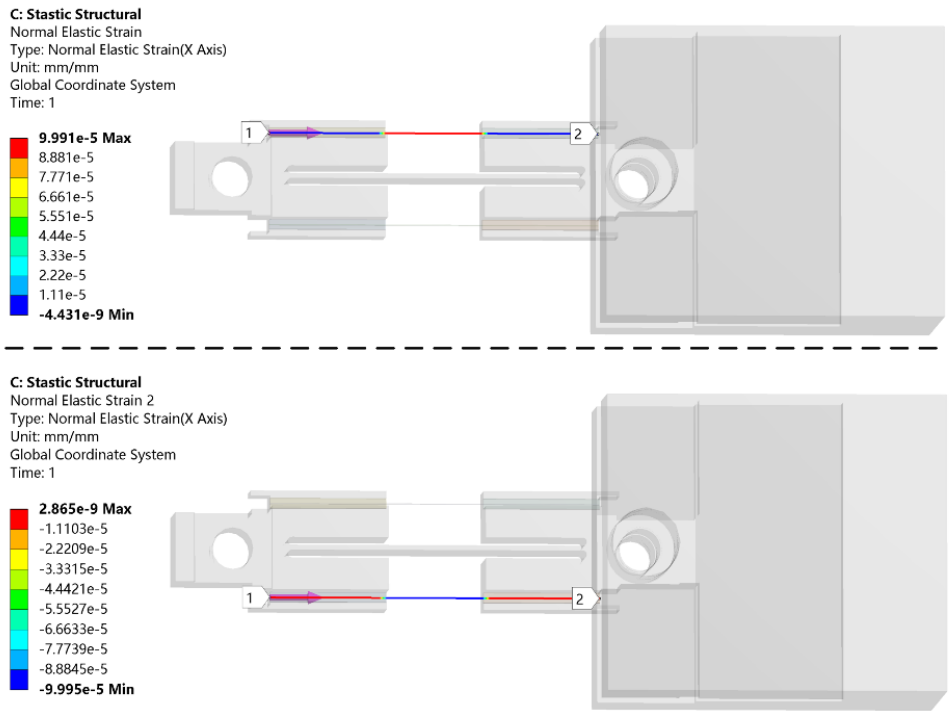

Fig. 6 Strain cloud of the tilt sensor.

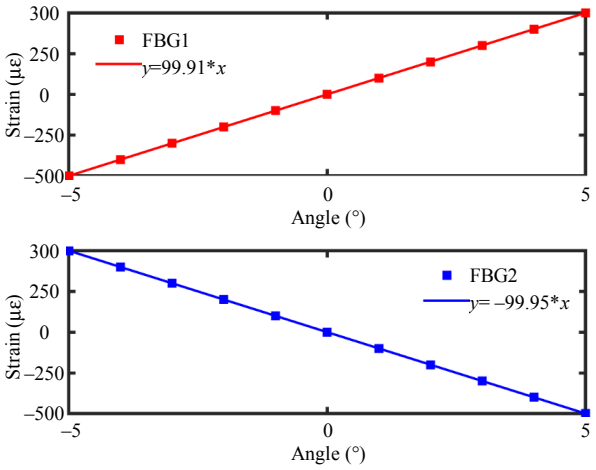

Fig. 7 Strain results of the simulation.

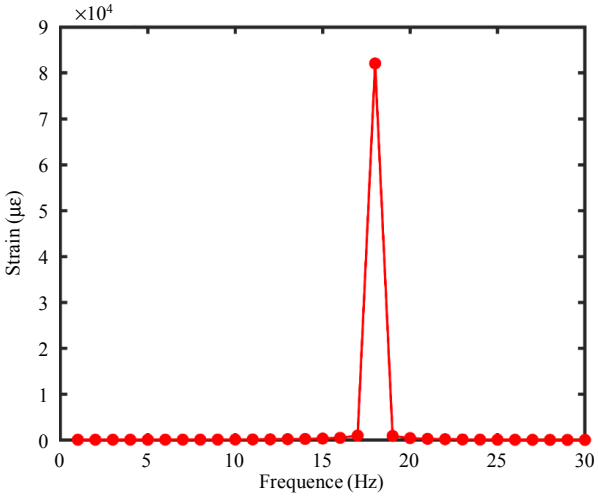

Fig. 8 Frequency response curve of the tilt sensor.

3. Experiments and results

3.1 Experiments

In order to study the performance of the sensor, the experimental setup is built, as shown in Fig. 9. The assembled sensor and piezoelectric inclinometer are mounted on an inclination platform, two FBGs are connected to the demodulator, and the demodulator is connected to a computer. The inclination platform is used to generate the tilt angle, the piezoelectric inclinometer is used to validate the tilt angle, the demodulator is used to demodulate the optical signal, and the computer is used to read the wavelength data. Before the experiment, the tilt angle of the inclination platform is adjusted to 0°, and the piezoelectric inclinometer is used for validation to ensure that the inclination platform is correctly placed on the horizontal platform, and the wavelength is recorded. After the experiment starts, a tilt angle of –5° to 5° with a step of 0.5° is applied through the inclination platform. To avoid the error caused by the change lag, stop at each tilt point for 5 seconds to 8 seconds. The experiment is cycled for 3 times, and the wavelengths of the two FBGs are collected and recorded with a sampling frequency of 10 Hz.

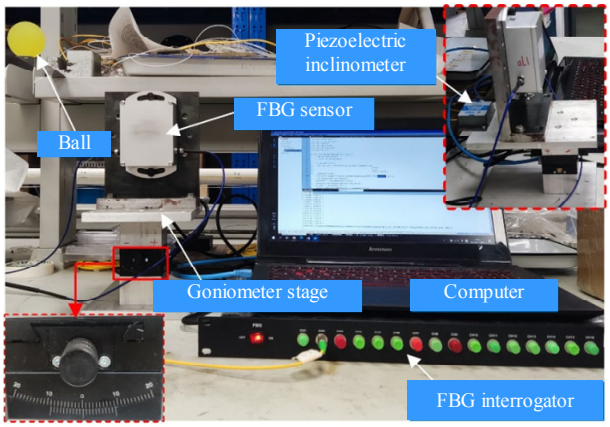

Fig. 9 Performance test platform of the sensor.

In some practical application situations, vibration usually occurs simultaneously with tilt, which puts forward higher requirements for the dynamic performance of the sensor. It can be seen from the simulation analysis that the frequency range satisfying the normal operation of the sensor is small, which means that the sensor is susceptible to random vibration. The silicone oil can be used as a vibration damping fluid because it has excellent shear stability and the function of absorbing vibration and preventing vibration transmission. Therefore, the experiment is designed to study the influence of the silicone oil on the seismic performance of the sensor. The sensor is fixed on the tilt platform and the tilt angle is calibrated to 0° using a piezoelectric inclinometer. In the first step, a ball is released freely near the sensor above the experimental platform. Sensors are excited after the ball hits the experimental platform. In the second step, the silicone oil with the viscosity of 500 pcs is injected into the shell of the sensor, and the same method is used to make sensors subject to excitation signals. To ensure that the sensor receives the same excitation signal, the release height and position of the ball are consistent in the two steps. The demodulator with the 1 000 Hz sampling frequency is used to collect the wavelength change data of an FBG during the experiment.

The FBG is sensitive to both the strain and temperature. Therefore, the temperature compensation ability of the designed sensor is studied. The sensor is placed in the temperature control box, the temperature is adjusted from 20 ℃ to 80 ℃, with a step of 10 ℃, and the wavelengths of the two FBGs are recorded.

3.2 Results and discussion

Figure 10 shows the relationship between the central wavelengths of the two FBGs and the tilt angle. The repeatability of the three experimental results is good, and the central wavelengths of the two FBGs have a good linear relationship with the tilt angle. Figure 11 shows the linear fitting results between the central wavelength difference and the tilt angle. The sensitivity of the sensor is about 231.7 pm/°, the errors with the theoretical

calculation and simulation results are 7.8% and 3.5%, respectively, and the coefficient of determination reaches 0.999 5. All these experimental data confirm that the proposed tilt sensor can achieve the high precision angle measurement.

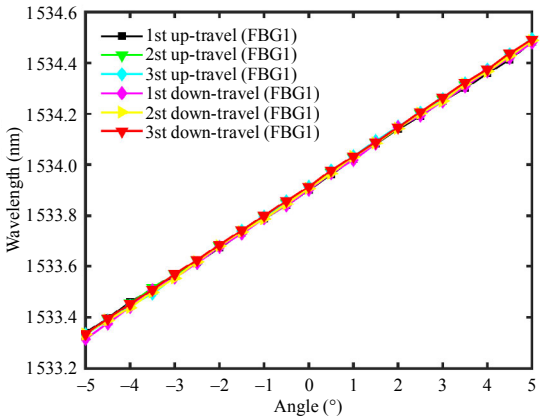

(a)

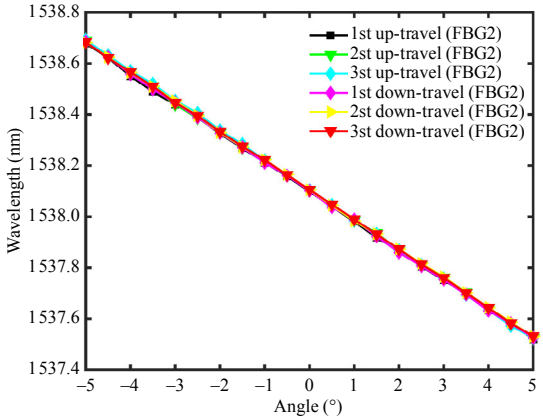

(b)

Fig. 10 Corresponding relationship between the wavelength shifts and tilt angle: (a) FBG1 and (b) FBG2.

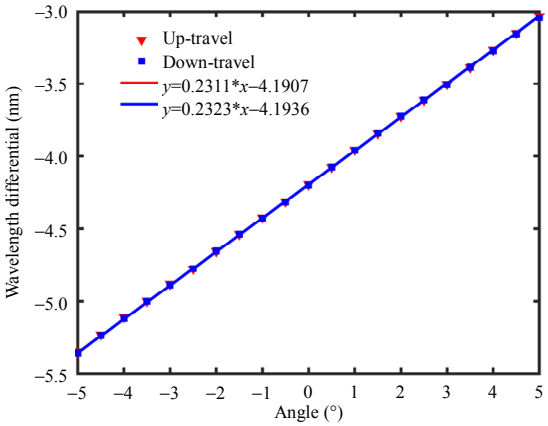

Fig. 11 Tilt sensitivity of the tilt sensor.

Figure 12 shows the time-history curve of the wavelength of an FBG when there is no silicone oil inside the shell. After the sensor receives the excitation signal provided by the ball, the time to restore the stable state is about 600 ms, and the maximum amplitude of the wavelength shift is about 168 pm. Figure 13 shows a time-history curve of the wavelength of an FBG after the silicone oil is injected inside the shell. When the sensor receives the same excitation signal, the time to restore the stable state is about 90 ms, and the maximum amplitude of the wavelength shift is about 45 pm. After sealing the silicone oil inside the shell, the time for wavelength recovery to a stable state and the amplitude of wavelength change are significantly reduced with the excitation signal provided by the ball, which shows the damping effect of the silicone oil is obvious.

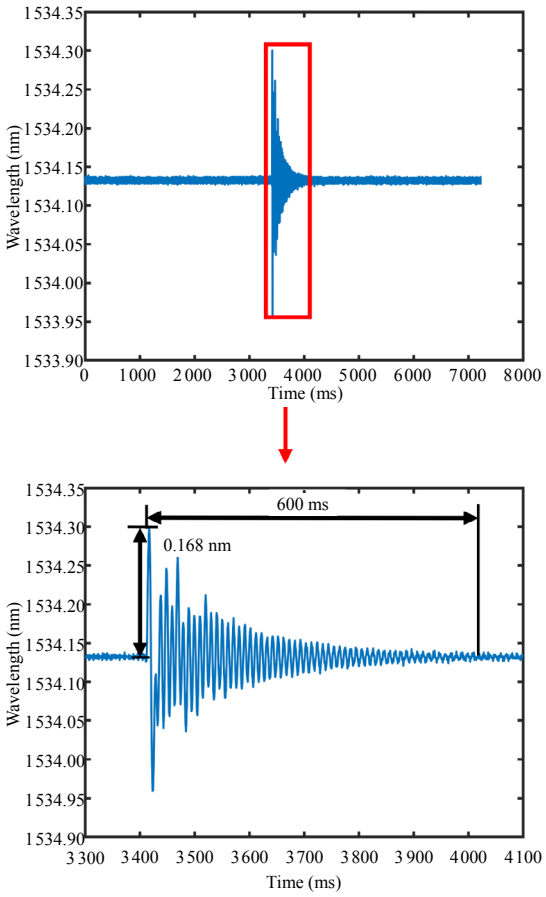

Fig. 12 Time-history curve of the wavelength without silicone oil.

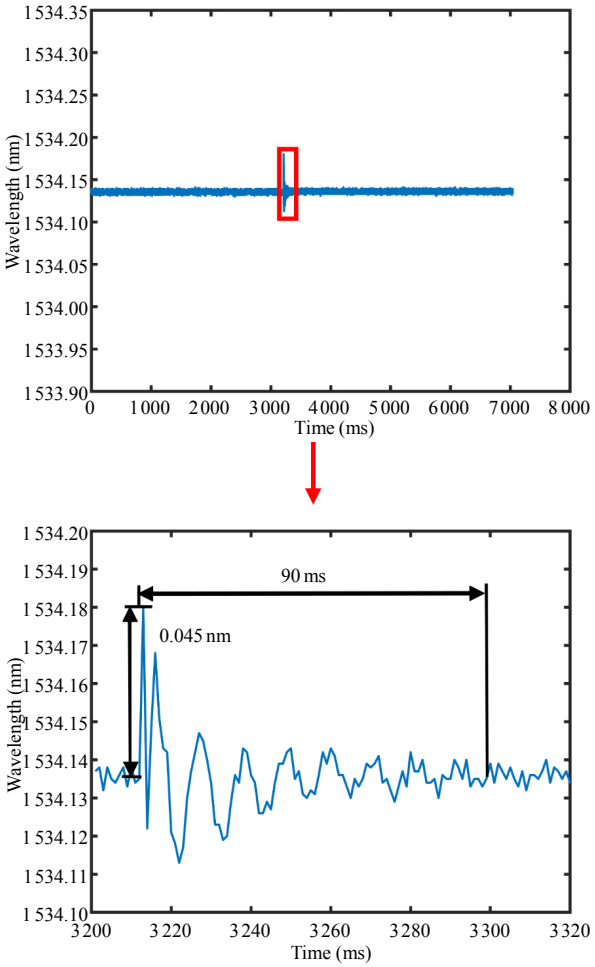

Fig. 13 Time-history curve of the wavelength with silicone oil.

Figure 14 shows the relationship between the wavelength shifts of two FBGs and the temperature. It can be found that the wavelength shifts of the two FBGs have a good linear relationship with the temperature, the temperature sensitivity of the two FBGs are 21.503 pm/℃ and 20.834 pm/℃, respectively, and the difference is small. Therefore, the effect of temperature on the measured tilt angle can be eliminated.

Table 3 compares the size of the main structure, sensitivity, and other performance indicators of the designed sensor with the previous reference. Obviously, the sensitivity of the designed sensor is higher than those of other sensors in the table. At the same time, its structural size also has an advantage. Therefore, it has a good application prospect in small inclination measurement of the conventional mechanical structure.

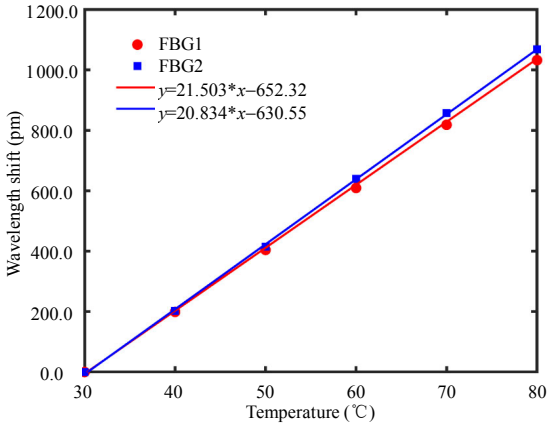

Fig. 14 Temperature responses of the tilt sensor.

Table 3 Performance comparison of FBG tilt sensors.

Lists	Tilt sensitivity (pm/°)	Measuring range (°)	Temperature self-compensation	Size
Jiang *et al.* [10]	9.9	–30 to 30	Yes	>35 mm (length)
Ma *et al.* [11]	16.17	–45 to 45	No	>50 mm (length)
Liang *et al.* [12]	31.3	–45 to 45	Yes	60 mm×20 mm× 20 mm
Yang *et al.* [15]	74	0 to 40	Yes	>380 mm (length)
Maheshwari *et al.* [16]	168	0 to 6	No	400 mm ×70 mm× 70 mm
Our work	231.7	–5 to 5	Yes	70 mm ×30 mm× 25 mm^2

4. Field testing

The proposed sensor is applied and tested on a pier of a subway viaduct in Shenzhen city, Guangdong province, China. The foundation pit construction is being carried out around the viaduct pier, and the protective monitoring of pier safety is needed. The horizontal displacement of the top of the viaduct pier is monitored by building a fiber optic sensing network, and the monitoring scheme and principle are shown in Fig. 15. Four tilt sensors are installed on the pier, and two are in a group: #1 and #3 sensors are used to monitor the tilt angle in the *x*-direction, and #2 and #4 sensors are used to monitor the tilt angle in the *y*-direction. Two sensors in the *x*-direction are taken as an example and in the *y*-direction, the same theory is used. One sensor is

installed at the waist of the bridge pier, 3 m away from the ground, and the other sensor is installed at the top of the bridge pier, 10 m away from the ground. When the pier is inclined, the horizontal displacement in the *x*-direction at the top of the pier can be expressed as

$$d = 3\,000\sin\theta_1 + 7\,000\sin\theta_2 \qquad (12)$$

where θ_1 is the tilt angle measured by the #3 sensor, and θ_2 is the tilt angle measured by the #1 sensor.

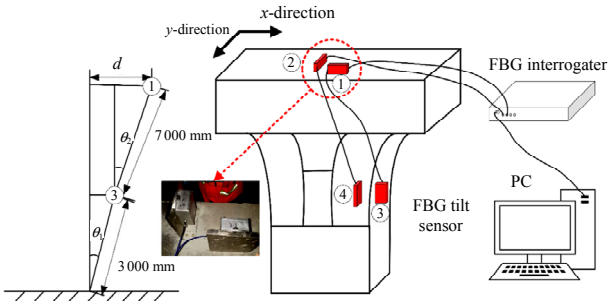

Fig. 15 Monitoring system and principle of the field test.

Figure 16 shows horizontal displacements in two directions at the top of the viaduct pier. During the monitoring period, the horizontal displacement of the two directions of the pier is small and locates in the safe range, indicating that the influence of foundation pit construction on the viaduct pier is small.

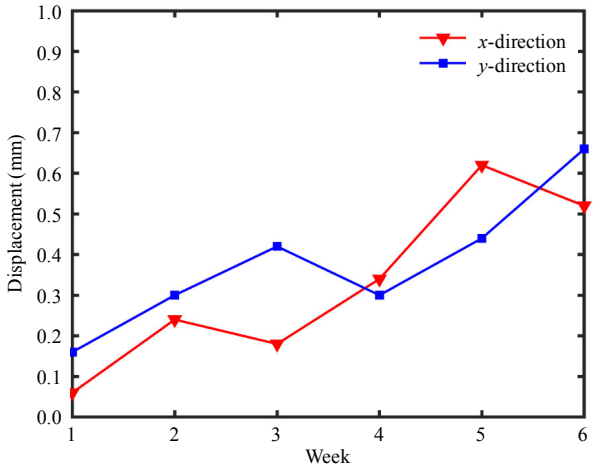

Fig. 16 Displacement curve during the monitoring period.

5. Conclusions

In this paper, a high-sensitivity FBG tilt sensor is introduced. The sensor with a cantilever-based structure achieves the high tilt sensitivity in the case of the small size compared with the traditional equal strength cantilever beam tilt sensor. The design and sensing principle of the tilt sensor are introduced in detail. The performance of the sensor is studied. The result shows that there is a good linear relationship between the central wavelength difference of the two FBGs and the tilt angle in the range of –5° to 5°, and the repeatability is good. The tilt sensitivity is 231.7 pm/°, and the resonant frequency of the sensor is about 18 Hz, which indicates that the sensor has a good application prospect in the small angle measurement under the low frequency environment. The influence of the silicone oil on the seismic performance of the sensor is studied. The results show that the sealing silicone oil inside the shell of the sensor can effectively reduce the influence of random vibration, which is of great significance to improve the reliability of sensors in practical engineering applications. The field test is carried out on the pier of an elevated bridge, and the monitoring results are satisfactory, which verifies the practicability of the proposed sensor in the inclination monitoring of the bridge.

Acknowledgment

This work was supported by the Fundamental Research Funds for the Central Universities (Grant No. 2019 III 158CG) and the National Natural Science Foundation of China (Grant No. 61875155).

References

[1] M. Majumder, T. K. Gangopadhyay, A. K. Chakraborty, K. Dasgupta, K. Dasgupta, and D. K. Bhattacharya, “Fibre Bragg gratings in structural

health monitoring – present status and applications," *Sensors and Actuators A – Physical*, 2008, 147(1): 150–164.

[2] F. I. H. Sakiyama, F. Lehmann, and H. Garrecht, "Structural health monitoring of concrete structures using fibre-optic-based sensors: a review," *Magazine of Concrete Research*, 2021, 73(4): 174–194.

[3] F. Xiao, G. S. Chen, and J. L. Hulsey, "Monitoring bridge dynamic responses using fiber Bragg grating tiltmeters," *Sensors*, 2017, 17(10): 2390.

[4] H. F. Pei, J. H. Yin, H. H. Zhu, C. Y. Hong, W. Jin, and D. S. Xu, "Monitoring of lateral displacements of a slope using a series of special fibre Bragg grating-based in-place inclinometers," *Measurement Science and Technology*, 2012, 23(2): 025007.

[5] C. Y. Hong, Y. F. Zhang, Z. Lu, and Z. Y. Yin, "A FBG tilt sensor fabricated using 3D printing technique for monitoring ground movement," *IEEE Sensors Journal*, 2019, 19(15): 6392–6399.

[6] N. L. Li, S. F. Jiang, M. H. Wu, S. Shen, and Y. Zhang, "Deformation monitoring for Chinese traditional timber buildings using fiber Bragg grating sensors," *Sensors*, 2018, 18(6): 1968.

[7] C. Y. Hong, Y. F. Zhang, M. X. Zhang, L. L. M. Gordon, and L. Q. Liu, "Application of FBG sensors for geotechnical health monitoring, a review of sensor design, implementation methods and packaging techniques," *Sensors and Actuators A – Physical*, 2016, 244: 184–197.

[8] H. B. Xu, X.Y. Zheng, W. G. Zhao, X. Sun, F. Li, Y. L. Du, *et al.*, "High precision, small size and flexible FBG strain sensor for slope model monitoring," *Sensors*, 2019, 19(12): 2716.

[9] Y. X. Guo, L. Xiong, and H. H. Liu, "Research on the durability of metal-packaged fiber Bragg grating sensors," *IEEE Photonics Technology Letters*, 2019, 31(7): 525–528.

[10] S. C. Jiang, J. Wang, and Q. M. Sui, "Distinguishable circumferential inclined direction tilt sensor based on fiber Bragg grating with wide measuring range and high accuracy," *Optics Communications*, 2015, 355: 58–63.

[11] G. M. Ma, C. R. Li, J. T. Quan, J. Jiang, and Y. C. Cheng, "A fiber Bragg grating tension and tilt sensor applied to icing monitoring on overhead transmission lines," *IEEE Transactions on Power Delivery*, 2011, 26(4): 2163–2170.

[12] M. F. Liang, X. Q. Fang, S. Li, G. Wu, M. Ma, and Y. G. Zhang, "A fiber Bragg grating tilt sensor for posture monitoring of hydraulic supports in coal mine working face," *Measurement*, 2019, 138: 305–313.

[13] G. W. Fu, J. Q. Cao, J. T. Zhang, X. H. Fu, W. Jin, and W. H. Bi, "An omni-azimuth angle sensor for tilt measuring based on FBG array," *IEEE Photonics Journal*, 2021, 13(6): 6800108.

[14] J. J. Pan, Q. M. Nan, S. J. Li, and Z. H. Hao, "Development of a high resolution optical-fiber tilt sensor by FP filter," in *2017 25th on Optical Fiber Sensors Conference (OFS), IEEE*, Korea, April, 2017, pp. 1–4.

[15] R. G. Yang, H. L. Bao, S. Q. Zhang, K. Ni, Y. Z. Zheng, and X. Y. Dong, "Simultaneous measurement of tilt angle and temperature with pendulum-based fiber Bragg grating sensor," *IEEE Sensors Journal*, 2015, 15(11): 6381–6384.

[16] M. Maheshwari, Y. W. Yang, D. Upadrashta, and T. Chaturved, "A rotation independent in-place inclinometer/tilt sensor based on fiber Bragg grating," *IEEE Transactions on Instrumentation and Measurement*, 2019, 68(8): 2943–2953.